Synthesis and Relationships between the Nonlinear Optical and Holographic Properties of Dual Functional Azocarbazole Chromophores Based on Photorefractive Polymers

Chi-Jung Chang and Wha-Tzong Whang*

Department of Materials Science and Engineering, National Chiao-Tung University, 1001 Ta Hsueh Road, Hsinchu 300, Taiwan, R.O.C.

Chia-Chen Hsu and Zhen-Yu Ding

Department of Physics, National Chung Cheng University, Ming-Hsiung, Chia-Yi, Taiwan, R.O.C.

Ken-Yuh Hsu and Shiuan-Huei Lin

Institute of Electrooptical Engineering, National Chiao-Tung University, 1001 Ta Hsueh Road, Hsinchu 300, Taiwan, R.O.C.

Received December 14, 1998

ABSTRACT: Two kinds of dual functional carbazole-based chromophores are synthesized to enhance the photorefractive (PR) performance of the polymers by attaching the electron-donating and electron-accepting groups with a diazo bridge on the 3- and 6-positions of the *N*-ethylcarbazole. The electron-donating group is *N*,*N*-diethanol aminophenyl. The electron-accepting group is either *p*-nitrophenyl or 5-nitrothiazole. The peak maximum of the UV/vis absorption spectra of the 5-nitrothiazole-containing chromophore PANTAC at 535 nm is longer than that of the *p*-nitrophenyl-containing PANPAC at 477 nm. Both chromophores exhibit a large first hyperpolarizability in the hyper-Rayleigh scattering experiment due to the extended chain length. The first hyperpolarizability of PANTAC is 1100×10^{-30} esu, almost the double of that of PANPAC (590×10^{-30} esu). The diffraction efficiencies of both polymers are the function of the film thickness and the laser beam wavelength with a maximum η_{max} at a thickness d_{max} between 15 and 23 μm. Surprisingly, the PANPAC-based PR polymer reveals a higher maximum diffraction efficiency (η_{max}) and better fringe of the stored holograms than the PANTAC-based PR polymer does. Both the PR polymers written/read by the green/red laser have greater η_{max} values than those written/read by the green/green laser. These phenomena are related to the balance between absorption and transmission of the laser beam through the PR polymer.

Introduction

Photorefractive polymers exhibit both photoconductivity and optical nonlinearity. They have attracted considerable attention due to their potential applications in optical computing, optical correlation, and three-dimensional data or image storage.[1−5] In general, the organic PR polymers can be classified into two types: doped polymers[6−10] and fully functionalized polymers in which the photoconducting moiety and the nonlinear optical chromophore are chemically bonded onto the polymer chains.[11−15] A large portion of the reported fully functionalized PR polymers are prepared by use of a backbone functionalized with separate charge generator, charge transporter, and nonlinear optical (NLO) chromophores. The NLO chromophore and the charge-transporting component compete for volume fraction in the PR polymer. They suffered from problems such as the dilution of each component by the others. However, the concentration of each functionality should be as high as possible to achieve a large diffraction efficiency and fast response. To overcome the previous problems, the PR polymer prepared from one single active component (dual functional chromophore) such as (dialkylamino)-nitrostilbene has been reported.[16] Ho et al.[17] reported a polymer with a pendent azo moiety on one side of the carbazole ring. The azo-containing carbazole groups provided both the photoconductivity and NLO activity, and the aliphatic chain attached on the N atom of the carbazole ring acted as the spacer.

The characteristics of the NLO chromophores may affect the PR properties of the PR polymers. The NLO chromophores are in general asymmetrically substituted molecules with an electron-donating moiety and an electron-accepting moiety separated by a conjugated structure. The common structure of the NLO chromophore is the involvement of benzenoid rings as the conjugated bridge Compared to the conjugated olefinic moieties, the benzenoid rings provide improved chemical stability to the compound. Several groups [18−23] even demonstrated that the conjugated molecules employing five-membered heterocyclic moieties possess superior second-order nonlinearity over molecules employing benzenoid moieties. Varanasi et al.[24] reported that the nonlinear response depended strongly not only on the nature but also on the location of the heterocyclic ring. Among the five-membered heterocyclic rings, pyrrole, furan, and thiophene are electron-rich, while thiazole, oxazole, and imidazole are electron-deficient in nature. The electron-rich or electron-deficient nature of the heterocyclic ring controls its response to the presence of additional substituents. In addition to the nature of heterocyclic rings, the β value can also be elevated by increasing the conjugation length in the heterocyclic system between the donor and the acceptor moieties.[25−28] However, the influence of introducing nonlinear optical

* To whom all correspondence should be addressed.

10.1021/ma981922d CCC: $18.00
Published on Web 07/30/1999

chromophores with different hyperpolarizability on the PR characteristics of the dual functional photorefractive polymer has not been studied.

In this paper, the relationships between the nonlinear optical and the holographic properties of the dual functional carbazole-based photorefractive polymers are studied. The hyper-Rayleigh scattering (HRS) technique is used to determine the β value of the dual functional chromophores. Flipse et al.[32] reported a discrepancy between the β values measured by HRS and by the electric field induced second harmonic generation (EFISH). It is mainly due to the two-photon absorption (TPA) induced Stokes and anti-Stokes fluorescence around the SH wavelength,[33] which is mixed with the HRS signal and makes β higher than those measured by EFISH. In this article, the TPA-induced fluorescence is measured and its contribution to the HRS β value is removed. We have tried to elevate the diffraction efficiency of the PR polymers in two ways. First, dual functional chromophores are used to maximize the concentration of each functionality. Second, the second-order optical susceptibility is promoted by extending the conjugation length with an additional electron-donating group and an additional electron-withdrawing group and/or introducing the five-membered heterocyclic ring onto the chromophore molecules. Since the carbazole molecule has a structure isoelectronic with diphenylamine, the reported dual functional carbazole-based fully functionalized PR polymers are all synthesized by introducing electron-withdrawing groups in the 3- and/or 6-positions to induce intracharge transfer and a dipole moment.[17,34,35] In this study, the dual functional carbazole-based fully functionalized PR polymers are synthesized by attaching additional electron-donating (dialkylamino)phenyl group and the electron-accepting nitrophenyl or nitrothiazole groups on the 3- and/or 6-positions of the carbazole ring by two consecutive diazo coupling reactions. It not only makes the chromophores dual functional but also makes the conjugation length longer than the published polymers. The influence of the electron acceptor of the chromophores on the PR characteristics and the resolution of the stored images in the dual functional PR polymers and their update capability for data storage are evaluated in this study.

Experimental Section

Materials. 3-Amino-*N*-ethylcarbazole (AEC) is chosen as the diazotization component. After being coupled with *N*,*N*-diethanol aniline, it is further coupled with the diazotized 4-nitroaniline and 2-amino-5-nitrothiazole to form the dual functional chromophores. (Scheme 1)

Scheme 1

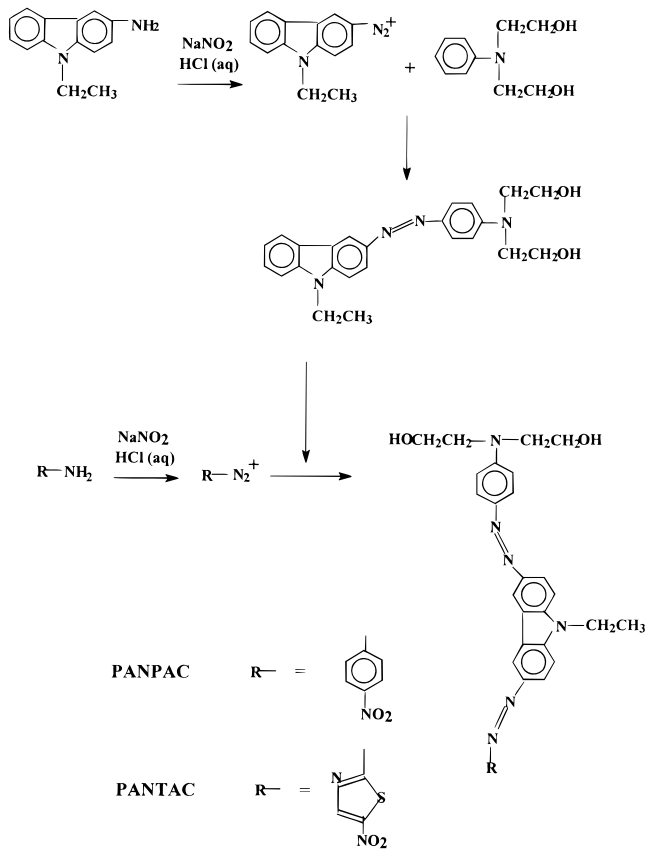

Preparation and Characterization of 3-{4-[*N*′,*N*′-Bis-(2-hydroxyethyl) amino]phenylazo}-*N*-ethylcarbazole (PAC). AEC (1.4 g, 0.0067mol) is dissolved in a solution of concentrated HCl (2 mL) in water (15 mL). The mixture is stirred and cooled in an ice bath until the temperature is below 4 °C. The 3-amino-*N*-ethylcarbazole hydrochloride is then separated off as a fine powder. The solution containing sodium nitrate (0.54 g, 0.0078 mol) in water is cooled below 4 °C and is added dropwise into the 3-amino-*N*-ethylcarbazole hydrochloride solution for diazotization in the ice bath with stirring for 40 min. *N*,*N*-Diethanolaniline (1.2 g, 0.0067 mol) in the concentrated HCl solution (1 mL) is added dropwise to the above mixture in the ice bath and stirred vigorously for 12 h. The resultant suspension solid is filtered and washed with water for several times to remove the residual HCl. The solid is vacuum-dried at 25 °C for 2 h to remove water and then recrystallized from ethanol/chloroform (2:1 by volume) to yield 1.8 g of 3-{4-[*N*′,*N*′-bis(2-hydroxyethyl)amino]phenylazo}-*N*-ethylcarbazole (PAC) (yield 70%). ^{1}H NMR (300 MHz, DMSO-d_6): δ 1.25 (t, 3H), 3.6 (m, 8H), 4.3 (q, 2H), 4.8 (t, 2H), 6.68 (d, 1H), 6.82 (d, 1H), 7.06 (t, 1H), 7.3 (d, 1H), 7.38 (t, 1H), 7.435 (d, 1H), 7.8 (d, 1H), 7.9 (d, 1H).

Preparation and Characterization of 3-{4-[N′,N′-Bis-(2-hydroxyethyl)amino]phenylazo}-6-(4-nitrophenylazo)-*N*-ethylcarbazole (PANPAC). 4-Nitroaniline (0.92 g, 0.0067 mol) is dissolved in a warm solution of concentrated HCl (2 mL) in water (8 mL). The mixture is stirred and cooled in an ice bath to 2−4 °C. The 4-nitroaniline hydrochloride is then separated out as a fine powder. The solution containing sodium nitrate (0.54 g, 0.0078 mol) in water (2.5 mL) is cooled below 4 °C and is added slowly into the 4-nitroaniline hydrochloride solution in an ice bath with stirring for 30 min. PAC (2.69 g, 0.0067 mol) is dissolved in a solution of 2 mL of concentrated HCl and 8 mL of water in an ice bath. The PAC solution is added dropwise to the previous mixture in the ice bath and stirred vigorously for 12 h. The resultant suspension solid is filtered and washed with water for several times to remove the residual HCl. The solid is vacuum-dried at 25 °C for 2 h and then recrystallized from ethanol/chloroform (2:1 by volume) to yield 1.98 g of 3-{4-[*N*′,*N*′-bis(2-hydroxyethyl)amino]-phenylazo}-6-(4-nitrophenylazo)-*N*-ethylcarbazole (PANPAC) (yield 52%) (HNPECD). ^{1}H NMR (300 MHz, DMSO-d_6): δ 1.3 (t, 3H), 3.4 (m, 8H), 4.4 (q, 2H), 4.7 (t, 2H), 6.65 (d, 2H, ArH), 6.9 (d, 2H, ArH), 7.05 (d, 2H, ArH), 7.04 (s, 2H, ArH), 7.8 (d, 2H, ArH), 7.9 (d, 2H, ArH), 8.4 (d, 2H, ArH). Anal. Calcd for $C_{30}H_{29}N_7O_4$: C, 65.32; H, 5.3; N, 17.77; O, 11.6. Found: C, 65.23; H, 5.53; N, 17.62; O, 11.67.

Preparation and Characterization of 3-{4-[*N*,*N*−Bis-(2-hydroxyethyl)amino]phenylazo}-6-(5-nitrothiazo-2-azo)-*N*-ethylcarbazole (PANTAC). This compound is synthesized in a procedure similar to that used for PANPAC except that 2-amino-5-nitrothiazole (0.97 g, 0.0067mol) is used instead of 4-nitroaniline in the previous procedure. A yield of 1.46 g of the PANTAC chromophore is obtained (40%).^{1}H NMR (300 MHz, DMSO-d_6): δ 1.0 (t, 3H), 3.5 (m, 8H), 4.4 (q, 2H), 5.0 (t, 2H), 6.6 (d, 2H, ArH), 6.8 (d, 2H, ArH), 7.05 (d, 2H,

Scheme 2

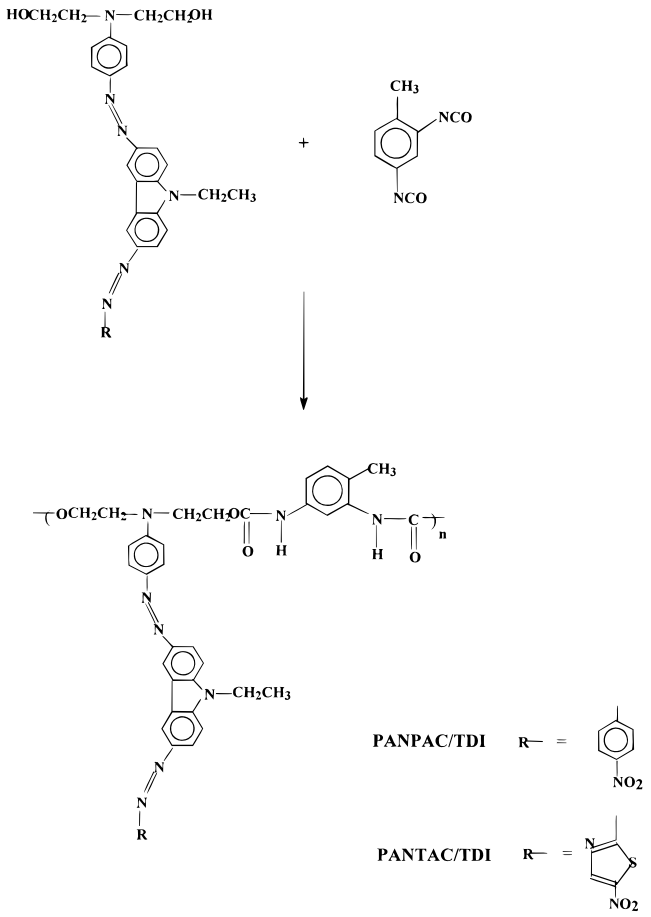

ArH), 7.04 (s, 2H, ArH), 7.8 (d, 2H, ArH), 8.8 (s, 1H). Anal. Calcd for $C_{27}H_{26}N_8O_4S$: C, 58.06; H, 4.66; N, 20.01; O, 11.47. Found: C, 57.67; H, 4.84; N, 18.03; O, 10.88.

Preparation of the PR Polymers. The polymers are prepared according to the reaction shown in Scheme 2.

TDI (0.25 g, 0.0015 mol) is added into the solution of PANPAC (0.83 g, 0.0015 mol) in cyclohexanone (8 mL). The solution is then refluxed at 105 °C for 10 h under nitrogen atmosphere. The resultant solution is dried under vacuum at 100 °C for 8 h to remove the residual solvent. The PR polymer is denoted as PANPAC/TDI. ^{1}H NMR (300 MHz, DMSO-d_6) δ 1.35 (t, 3H), 2.3 (s, 3H), 3.4−3.8 (m, 8H), 4.2−4.6 (m, 4H), 6.8−8.4 (m, 17H, ArH).

TDI (0.25 g, 0.0015 mol) is added into the solution of PANTAC (0.84 g, 0.0015 mol) in cyclohexanone (8 mL). The solution is refluxed at 105 °C for 10 h under a nitrogen atmosphere. The resultant solution is dried under vacuum at 100 °C for 8 h to remove the residual solvent. The PR polymer is denoted as PANTAC/TDI. ^{1}H NMR (300 MHz, DMSO-d_6): δ 1.2 (m, 3H), 2.4 (s, 3H), 3.3−3.7 (m, 8H), 4.2−4.6 (m, 4H), 6.4−8.0 (m, 13H, ArH), 8.8 (s, 1H).

After the solvent is removed from the polymer solution, the dried polymer is grounded into fine powder. The polymer in cyclohexanone is spin-coated onto the ITO side of an ITO glass and then dried under vacuum at 110 °C for 3 h to form the thin PR polymer film.

Measurements. The optical nonlinearity of the dual functional carbazole chromophore is measured by the HRS method. Although EFISH is the most common technique for determining the molecular first hyperpolarizability (β) of organic chromophores,[29,30] a dc external electric field is necessary to create a noncentrosymmetric environment in the EFISH method. Such an external electric field makes the data analysis more complicated because the ground-state dipole moment, the second hyperpolarizability, and the local field correction factor are required for the β measurement. Recently, HRS has been demonstrated to be a useful and simpler method to characterize the β value. The second harmonic (SH) signal in the HRS measurement occurs as a result of fluctuations in both the number density and the orientation of chromophores in the subvolumes in the active region of the solution.[31] These fluctuations distort the local symmetry among the subvolumes. Therefore, no dc electric field is required to distort the isotropy of the solution. Irradiate the solution by a laser beam with the frequency ω, and the scattered photons at frequency 2ω are detected.

In the HRS experiment, a Q-switched Nd:YAG laser generating 8 ns pulses with a 10 Hz repetition rate at 1064 nm is used as the light source. The incident laser intensity is modulated by rotating a computer-controlled half wave plate between a pair of polarizers. After passing through high pass filters to block short-wavelength flash noise, the laser beam is focused on the sample in a glass cylindrical cell (radius 1.25 cm) by a lens. The scattered light is collected by an aspheric lens at a scattering angle 90°. The collected light first passed through an interference band-pass filter and two low pass filters to ensure that only the 532 nm light can be detected by the photomultiplier tube (PMT) with a biased around 1200 V. A boxcar integrator is used to integrate and to digitize both the fundamental and the hyper-Rayleigh signals from the fast photodiode and the PMT, respectively. Every data point is the average of 300 laser shots.

Degenerate four-wave mixing (FWM) experiment is used to measure the PR properties. A green beam laser (λ = 514 nm) and a red beam laser (λ = 632.8 nm) are applied as the writing and reading beam, respectively. Two mutually coherent s-polarized writing beams are spatially overlapped in the polymer film with an angle (20°) to form a diffraction grating. A p-polarized reading beam is counterpropagating to one of the writing beams at the Bragg matching condition. The diffracted signal is detected by a photodetector.

The experimental setup for the holographic recording and readout is demonstrated in Figure 1. The image is written and read by a green light laser (λ = 532 nm). During holographic recording, the beam is expanded by a beam expander and then split into two writing beams, beam 1 and beam 2, by a beam splitter. Both writing beams are s-polarized. Beam 1 illuminated the center part of a image chart, and then the pattern is imaged onto the photorefractive polymer film. Beam 2 is incident on the polymer film at an incident angle of 30°. The average power density measured at the polymer plane is about 14 mW/cm^2. After the hologram is recorded, beam 1 is cut, and the hologram image is readout by beam 2. The restored image is detected by a CCD camera. The recorded image is erased by beam 2 over long time exposure. The same spot of the PR polymer is overwritten by using a new image chart under the interferent exposure of beam 1 and beam 2. The hologram recording lasts for 30 min without applying an electric field.

The DSC data are measured with a DuPont 2910 Thermal Analysis System at a heating rate of 10 °C/min. The UV/vis spectra are obtained with a Hitachi-U2000 spectrometer.

Results and Discussion

Characterization. The syntheses of all monomers and polymers are performed as described in the reaction scheme. The amino group on the 3-position of the carbazole ring allowed these two diazo coupling reactions to proceed step by step. Two novel types of carbazole-based dual functional chromophore are synthesized, different from other reports with only an electron acceptor bonding onto the carbazole ring. In our study, electron-donating and electron-withdrawing substituents are chemically bonded onto the 3- and 6-positions of the carbazole ring through an azo-conjugated bridge. To promote the yield of the PANTAC chromophore, PAC should be added as soon as possible once the 2-amino-5-nitrothiazole is diazotized. ^{1}H NMR spectra and elemental analysis data of PANPAC and

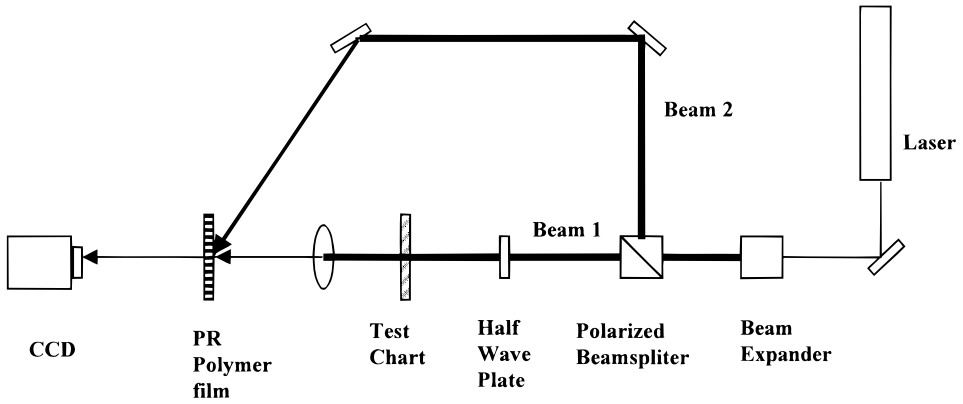

Figure 1. Experimental setup used for the holographic recording and readout.

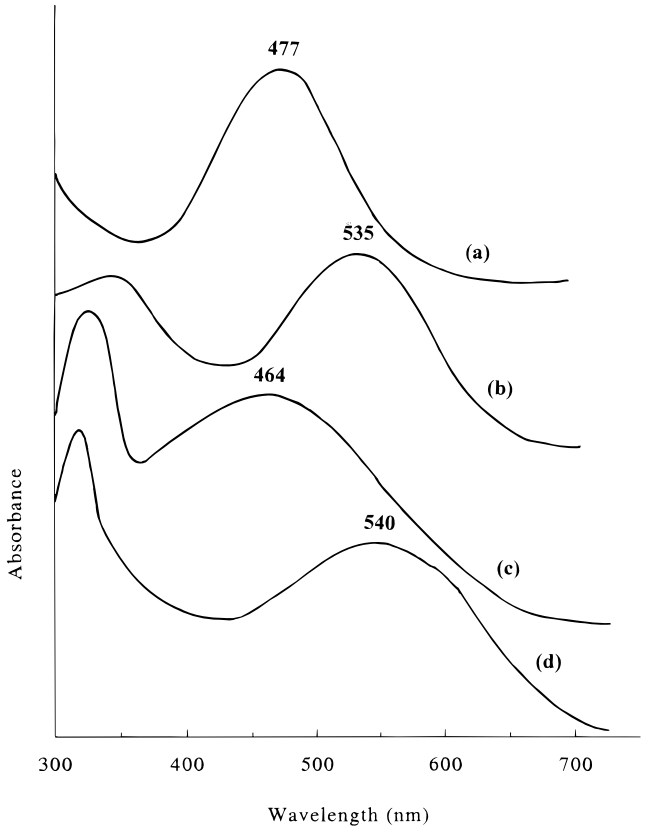

Figure 2. UV/vis absorption spectra of (a) PANPAC in dioxane, (b) PANTAC in dioxane, (c) PANPAC/TDI film, and (d) PANTAC/TDI film.

PANTAC shown in the Experimental Section match the chemical structure of the samples.

The UV/vis absorption spectra of monomers and the polymer are displayed in Figure 2. The wavelengths of the absorption maxima (λ_{max}) of the PANPAC and PANTAC chromophores in 1,4-dioxane are 477 and 535 nm, respectively. The typical absorption peak of AEC is located at 350 nm. The maximum absorptions of PANPAC/TDI and PANTAC/TDI polymers are located at 464 and 540 nm, respectively. The wavelength of the absorption peak of the PANTAC/TDI PR polymer is closer to the wavelength of the writing beams (514 nm) than that of PANPAC/TDI. The λ_{max} values of both chromophore **1** and **2** are higher than that of the azocarbazole reported by Ho et al. because extending the conjugation length by two consecutive coupling reaction results in a longer π- electron delocalization.

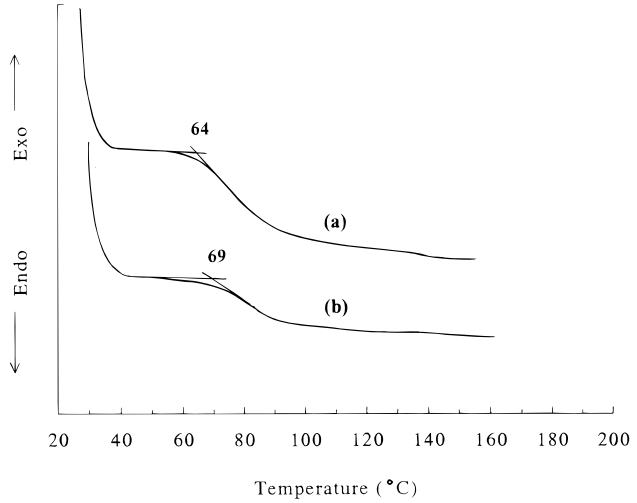

Figure 3. Differential scanning calorimetry (DSC) curves of (a) PANPAC/TDI polymer and (b) PANTAC/TDI polymer.

Differential scanning calorimetry (DSC) diagrams of different PR polymers are illustrated in Figure 3. The glass transition temperatures (T_g) of PANPAC/TDI and PANTAC/TDI films lie at 64 and 69 °C, respectively.

Nonlinear Optical Properties. Figure 4 shows the narrow HRS and broad TPA-induced fluorescence spectra of PANPAC and PANTAC in dioxane. The substructure of the TPA-induced fluorescence spectra which is found away from the wavelength of the HRS signal, has been smoothed out. In comparison with the TPA-induced fluorescence, the HRS signals at 532 nm are weak but distinguishable. Assuming the TPA-induced fluorescence has no substructure at 532 nm, the ratio of the TPA-induced fluorescence to the HRS signal at 532 nm can thus be obtained. From the ratio, the contribution of the TPA-induced fluorescence to the HRS β value is removed.

The HRS intensity $I_{2\omega}$ from a two component solute−solvent system at very low chromophore concentration is proportional to the square of the incident laser intensity I_ω:[31,33]

$$I_{2\omega} = G(N_s\beta_s^2 + N_c\beta_c^2)I_\omega^2 \quad (1)$$

Subscripts s and c stand for solvent and chromophore, respectively. N is the number density of the chromophore molecules. G is a constant related to the local field correction factor, the scattering geometry, and other optical and instrumental quantities.

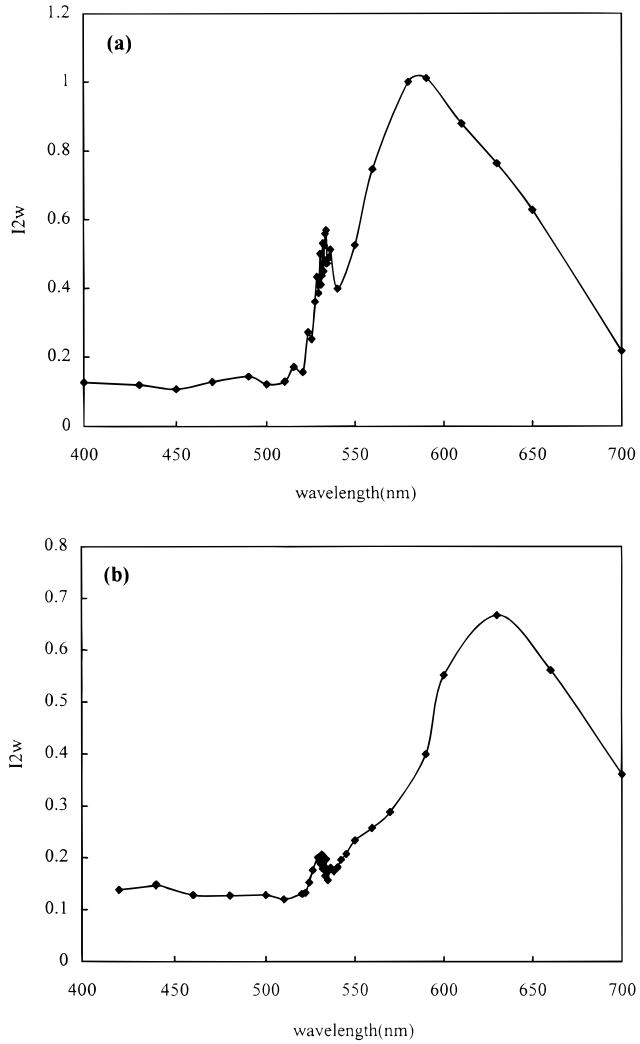

Figure 4. Two-photon absorption induced fluorescence spectra and HRS signals of (a) PANPAC in dioxane (b) PANTAC in dioxane.

The incident laser intensity I_ω is expressed as a function of the half-wave plate angle ϕ.

$$I_\omega = I_o \sin^2(2\phi + \alpha) \tag{2}$$

Here, I_o is the maximum intensity of the incident laser beam, and α is the start angle of the half-wave plate rotation.

Thus, $I_{2\omega}$ can be expressed as a function of ϕ as follows:

$$I_{2\omega} = I[\sin^4(2\phi + \alpha)] + b \tag{3}$$

Here, $I = Gk(N_s\beta_s^2 + N_c\beta_c^2)I_o^2$

Figure 5 shows the measured $I_{2\omega}$ of PANPAC in dioxane at 532 nm (circles) vs the half-wave plate angle. The solid line is generated with the eq 3. Since the experimental data is well fitted to eq 3, it reveals that the signals measured at 532 nm are due to the two-photon scattering process including both the HRS signals and TPA-induced fluorescence.

Since the HRS signals are absorbed by both chromophores, the detected HRS signals are attenuated by absorption. Correction of the HRS signal for absorption is necessary to calculate the correct β value.

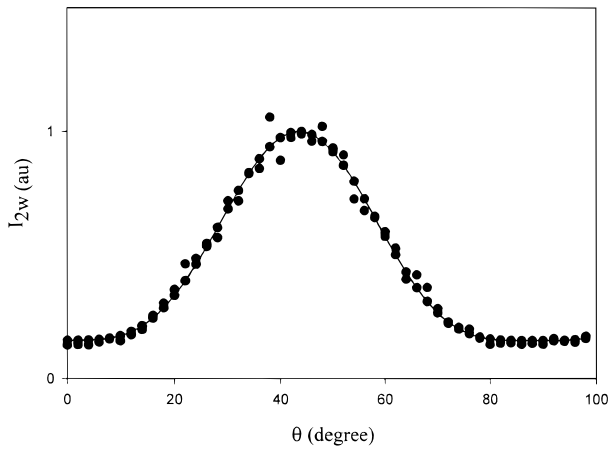

Figure 5. HRS intensity measured at 532 nm (circles) vs the half-wave plate angle (θ) for PANPAC in dioxane. The solid lines are the theoretical fit of eq 3 to the experimental data.

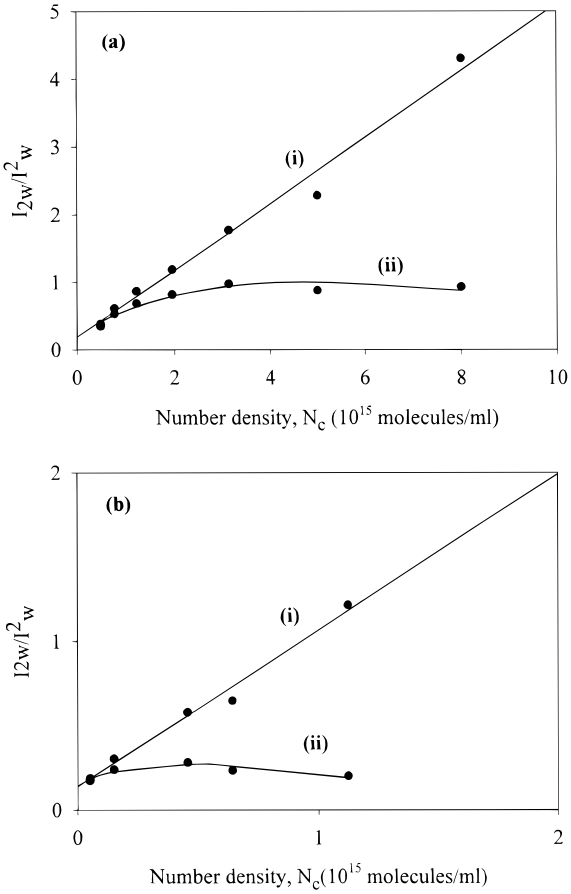

Figure 6. Plots of (i) corrected and (ii) uncorrected HRS signals vs the number density of (a) PANPAC in dioxane and (b) PANTAC in dioxane. The solid lines represent the theoretical fit to the experimental data.

The correction is made according to the following equation:

$$IR' = (IR)\exp(\epsilon N_c l) \tag{4}$$

Here, ϵ is the extinction coefficient of the chromophore in solution at the second harmonic wavelength. l is the effective path length that the $I_{2\omega}$ light travels. As shown in Figure 6, the uncorrected experimental data shows a curvature. The absorption effect can be eliminated by fitting the experimentally measured data to eq 4, and

Table 1. Absorption Maxima (λ_{Max}), First Hyperpolarizability (β_c), and Diffraction Efficiency (η_{Max}) of the Dual Functional Chromophores PANPAC, PANTAC, and Related Polymers Written/Read by Different Laser Beams

	λ_{max} (nm)	β_c (10^{-30} esu)	writing beam	reading beam	η_{max}	d_{max} (μm)
PANPAC	477	590				
PANTAC	535	1100				
PANPAC/TDI film	475		green	green	9.0×10^{-4}	23
PANTAC/TDI film	540		green	green	5.2×10^{-5}	15
PANPAC/TDI film	475		green	red	5.0×10^{-3}	22
PANTAC/TDI film	540		green	red	2.1×10^{-3}	17

a linear plot of the ($I_{2\omega}/I_{\omega}^2$) vs N_c for each solution is obtained.

Then, the external standard method is used to determine the hyperpolarizability of the chromophores β_c.

$$\beta_c = \beta'_c \sqrt{\frac{m_c}{m'_c}} \tag{5}$$

m_c and m'_c are the fitted slopes of the I vs N_c plots for the sample chromophore and the external standard solution, respectively. *p*-Nitroaniline (PNA) in dioxane solution with a known β value of 16.9×10^{-30} esu is used as the external standard. β_c values for PANPAC and PANTAC after removing the contribution of the TPA-induced fluorescence are 590×10^{-30} and 1100×10^{-30} esu, respectively. The nonlinear optical (NLO) properties of materials depend on the intramolecular transfer of electron density. The β_c of PANPAC is about 35 times as large as that of PNA due to extending the conjugation length. Because thiazole is an electron-deficient heterocyclic ring, even more electron deficient than oxazole and imidazole, the appearance of the thiazole ring at the acceptor end favors promotes the electron-withdrawing ability of the nitro group. It accounts for why the β_c of the PANTAC chromophore is almost twice as that of the benzene ring analogue PANPAC.

Photorefractive Properties. FWM measurement is used to study the photorefractive properties of the PR polymer films. The λ_{max} (UV/vis absorption), β_c, and η_{max} values of films written and read by different light sources are listed in Table 1, in which "the green laser" and "the red laser" represent the laser ($\lambda = 532$ nm) and the He−Ne laser ($\lambda = 632$ nm), respectively. The diffraction efficiency is dependent on the absorption of the reading beam by the film and on the film thickness. On the basis of the Kogelnik coupled wave model,[36] the diffraction efficiency η of the photorefractive grating can be given by

$$\eta = e^{-\alpha d} \sin^2(\pi d \Delta n/\lambda) \tag{6}$$

where α, d, and Δn are the absorption coefficient, the film thickness, and the effective refractive index change of the film, respectively. λ is the wavelength of the incident light. This equation shows that there is a maximum diffraction efficiency at a certain thickness. The maximum $\eta(\eta_{max})$ can be achieved by equating the following derivative to zero:

$$(\partial\eta/\partial d)_{\alpha,\Delta n} = 0 \tag{7}$$

From eq 6 and eq 7, there is maximum η_{max} at a certain film thickness (d_{max})

$$\tan(\pi d_{max} \Delta n/\lambda) = (2\pi\Delta n)/(\lambda\alpha) \tag{8}$$

$$\eta_{max} = e^{-\alpha d_{max}} \sin^2(\pi d_{max} \Delta n/\lambda) \tag{9}$$

After the film thickness is measured, α could be derived when the UV/vis spectrum is measured. Then, Δn could be calculated from eq 6 once η is measured from the FWM experiment. The dependence of η on d is calculated from eq 6. Parts a and b of Figure 7 show the plots of theoretical and experimentally measured diffraction efficiencies for PANPAC/TDI and PANTAC/TDI films written/read by the green laser vs different film thickness. As the film thickness increases, the theoretical curve increases at first and then drops later. The experimentally measured diffraction efficiencies of the films reach their maxima (η_{max}) 9×10^{-4} and 5.2×10^{-5} at the thickness (d_{max}) 23 and 15 μm, respectively. However, the latter decreases more rapidly than the former when the thickness is larger than d_{max}. It reveals that the equation is valid in thin films ($d < d_{max}$) only. When the film gets thicker, the absorption effect on the result of the experiment becomes more profound than that predicted by the equation. Parts c and d of Figure 7 show the plots of theoretical and experimentally measured diffraction efficiency of PANPAC/TDI and PANTAC/TDI films written/read by the green/red lasers vs different film thickness. The maximum diffraction efficiencies, 5.0×10^{-3} and 2.1×10^{-3}, of both polymers are located at film thickness of 22 and 17 μm, respectively. The absorption of the reading beam and the diffracted beam at 532 nm is stronger than at 632 nm. The diffraction efficiency shown in parts c and d decrease more slowly than those illustrated in parts a and b when the thickness is larger than d_{max}.

Although the β_c of PANTAC is almost twice as that of PANPAC, η_{max} of PANTAC/TDI written/read by the green/red laser is just half as much as that of PANPAC/TDI. As shown in Figure 2, the green laser wavelength 532 nm is located at the shoulder of the PANPAC/TDI absorption curve but at the peak of the PANTAC/TDI absorption curve. However, the red laser wavelength 632 nm is located at the valley of the former but at the shoulder of the latter. When the PR films are written and read by the green laser, the maximum diffraction efficiency of PANTAC/TDI is just 7% of that of PANPAC/TDI and the maximum diffraction efficiencies are lower than those written/read by the green/red laser. The maximum diffraction efficiencies of the PANTAC/TDI and PANPAC/TDI film written/read by the green/green laser are 17% and 2.5% of those written/read by the green/red laser. It is due to the absorption of both the reading beam and the diffracted beams (either green or red) by the PANTAC/TDI polymer, which are much stronger than the absorption by the PANPAC/TDI polymer. To exhibit photorefractive properties, an appropriate absorption by the PR material at the wavelength of the applied laser is necessary. Then, enough charge carriers can be generated and at the same time the diffracted light can be transmitted through the film without too much absorption by the polymeric material. It indicates that keeping the reading laser wavelength a proper distance from the absorption maximum of the

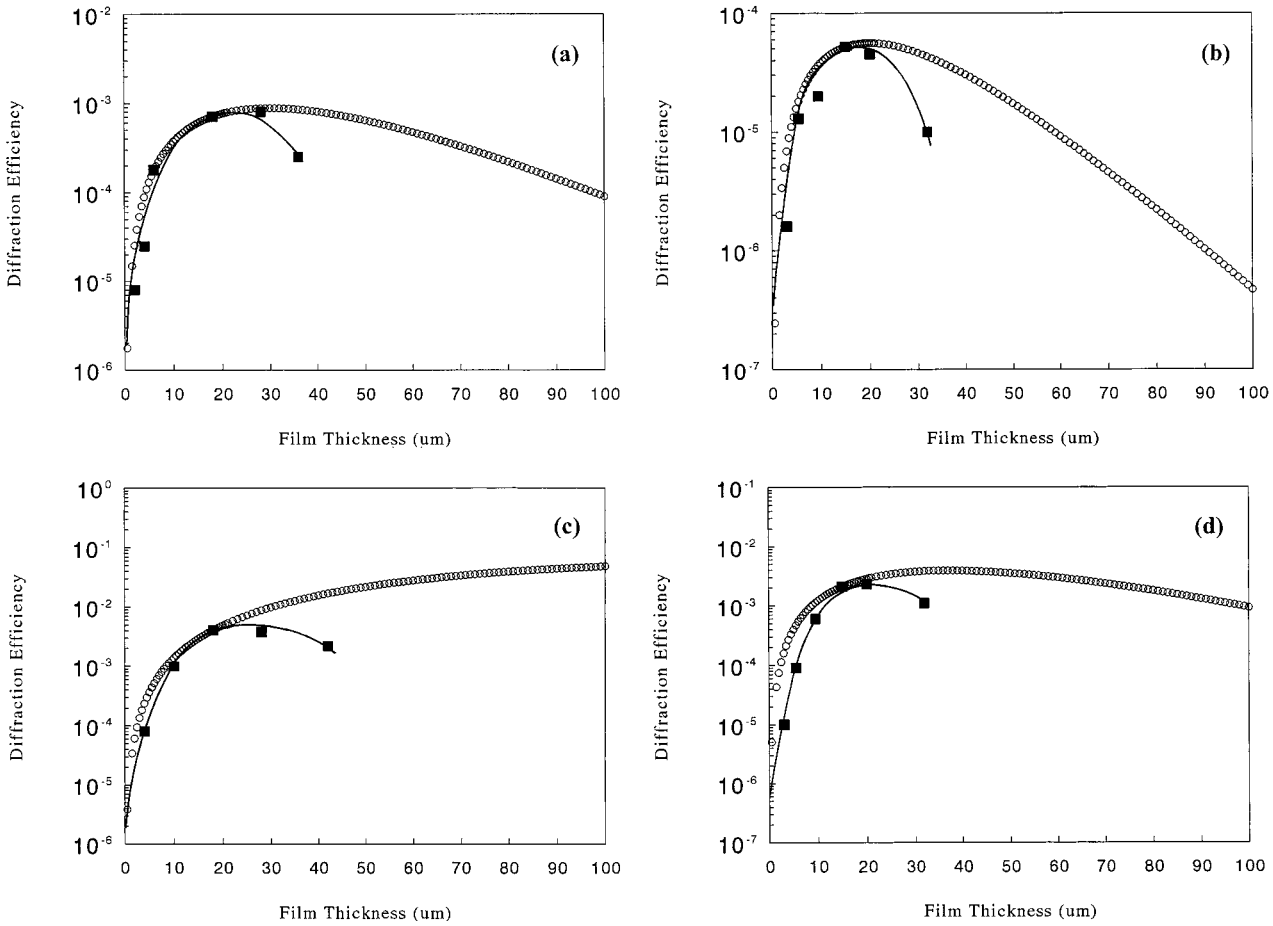

Figure 7. Plots of theoretical (open circles) and experimentally measured (filled squares) diffraction efficiency of (a) PANPAC/TDI, (b) PANTAC/TDI written/read by the green laser, (c) PANPAC/TDI, and (d) PANTAC/TDI written/read by the green/red lasers vs different film thickness.

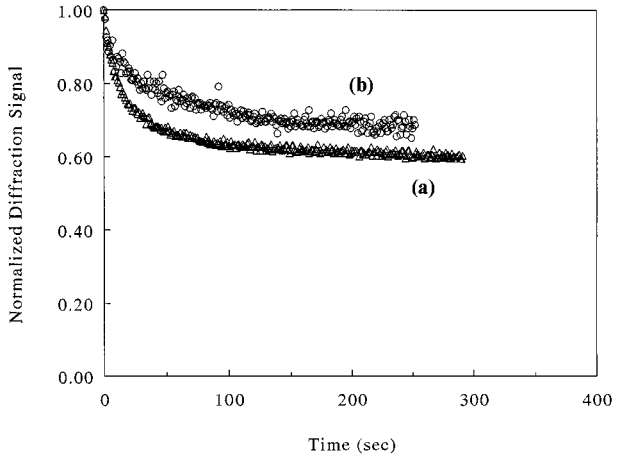

Figure 8. Dark decay of PR gratings in (a) PANPAC/TDI and (b) PANTAC/TDI.

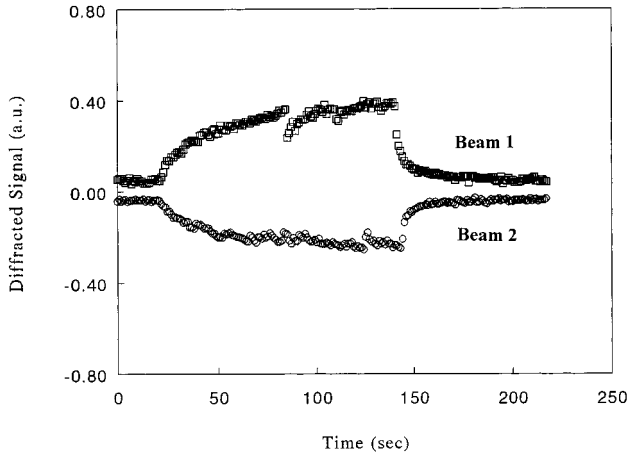

Figure 9. Asymmetric two-beam coupling of the PANPAC/TDI film.

film is helpful to promote diffraction efficiency. Usually, introducing NLO moieties with a large first hyperpolarizability will lead to a red shift in the UV/vis spectra. Therefore, both the λ_{max} in the UV/vis spectrum and the first hyperpolarizability β should be taken into account in designing new chromophores for the PR purpose.

The dark decay of the PR signals as a function of time at room temperature is illustrated in Figure 8. The PR signals of both films tend to decay to a stable value after a sharp initial decay. The PANTAC/TDI film with heteroaromatic ring retains higher percentage of its initial PR signal (70%) than the PANPAC/TDI film did (61%). It is attributed to the former having a higher T_g than the latter because both films contain the same main chain structure and the similar conjugation length.

Asymmetric two-beam coupling of the PANPAC/TDI film is shown in Figure 9. Samples had been previously irradiated to produce deep trap sites in the polymer which can enhance the modulated space charge field. It is a process refers to the optical trap activation. An increase in the intensity of beam 1 is observed after beam 2 is blocked. It is complemented by a decrease in the intensity of beam 2 when beam 1 is blocked. The

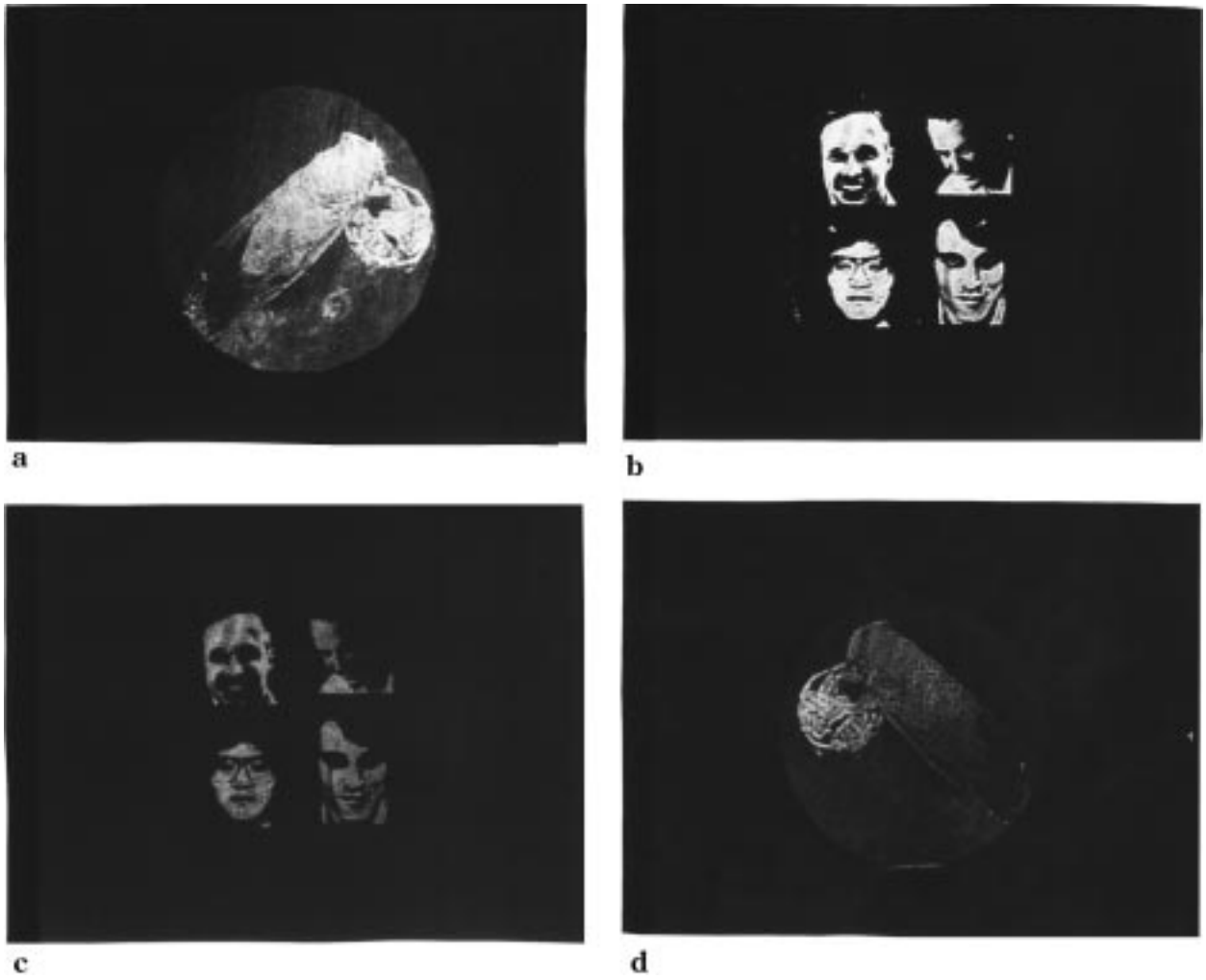

Figure 10. (a) Reconstructed image of a cicada (a familiar insect in Taiwan) standing on the cross section of a branch written in the PANPAC/TDI film. (b) Overwritten image of four portraits, (c) Dark decay after 1 h. (d) Same image as in part a written in the PANTAC/TDI film.

two-beam coupling performance confirms the sample films photorefractive.

Holographic Recording. To examine the potential application of the carbazole-based PR polymer on data or image storage, images are stored, erased, and overwritten on the same spot of the TDI/PANPAC film to investigated the erasure and update capability. A green laser ($\lambda = 532$ nm) is used as the writing and reading light source. In Figure 10a, a picture of a cicada (a familiar insect in Taiwan) standing on the cross section of a branch (mask 1) is recorded to demonstrate the film's performance in image storage. A clear image is observed. The recorded image is then deleted by continuously illuminating beam 2. Then, a new mask of four portraits (mask 2) is used to overwrite a new image on the same spot. The updated image is read and shown in Figure 10b. It shows that the PR polymer is rewritable and is a good hologram recording media since the images can be stored, erased, and updated repeatedly. To investigate the dark decay of the recorded holograms, a reconstructed image of mask 2 kept in the dark for 1 h is read as shown in Figure 10c. The quality of the image is retained except that the brightness is a little bit darker. In comparison with the images stored in the PANPAC/TDI film, the mask of the cicada is rotated 180° and recorded on the PANTAC/TDI film. The reconstructed image is shown in Figure 10d. Although the PANTAC chromophore possesses a larger β value than the PANPAC chromophore, the diffraction efficiency of the PANTAC/TDI film is lower than that of the PANPAC/TDI film written/read by the green/red laser. The image recorded on the PANTAC/TDI film is darker and more vague than those written in the PANPAC/TDI film. Since the absorption maximum of the PANTAC/TDI film shows a strong absorption on the green or red reading beams, the strong absorption on the diffraction signal leads to the poor quality of the recorded image. Strong absorption of the transmitted diffraction light is an inherent drawback for hologram storage. It confirms that keeping a proper distance between the absorption maxima of the films and the wavelength of the laser beam is helpful in promoting the resolution of the hologram.

A resolution test chart is utilized to evaluate the resolution of the recorded hologram images in the PR films. The chart consists of several groups of lines with different width and is correspondent to the USAF 1951 resolution target standard except for the group number. For example, the fifth group in this test chart is equal to the third group of the USAF resolution target standard, and the fourth group in this test chart is equal to the second group of the USAF resolution target standard, etc. Figure 11a shows the image of the original resolution chart transmitting through a filter. The lines are bright and the outlines are clear. Figure 11b illustrates a reconstructed image of the resolution

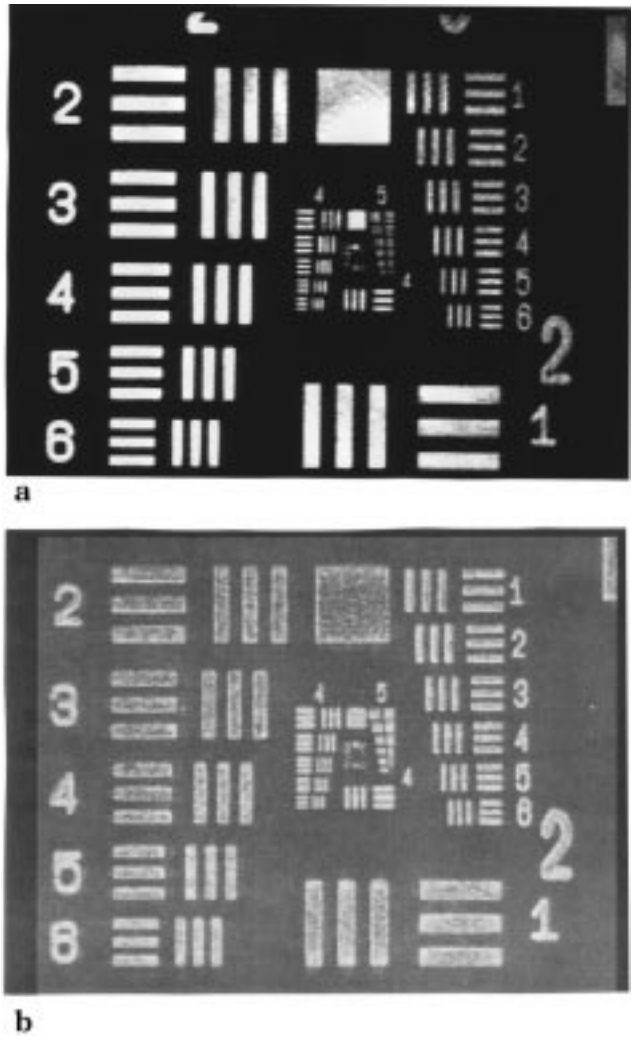

Figure 11. (a) Image of the original resolution chart transmitting through a filter and (b) a reconstructed image of the resolution chart written in the PANPAC/TDI film.

chart which is written in the PANPAC/TDI film. In Figure 10a, the fourth element of the fifth group is distinguishable. The corresponding element is perceptible in the restored image, as shown in Figure 11b. However, the outlines are more vague and the brightness of the lines are less than those in Figure 11a. It may be a result of the absorption of the diffracted signal. Taking the image demagnification in our optical system into account, the resolution of the recorded hologram is about 20 μm.

Conclusions

Two new types of dual functional carbazole-based polymers, PANPAC/TDI and PANTAC/TDI, are synthesized with electron-donating and electron-withdrawing substituents attaching on the 3- and 6-positions of the carbazole ring through an azo-conjugated bond, respectively. In the HRS experiment, the NLO signal can be separated from the fluorescence signal and is proved to be the second harmonic NLO response. Using the external standard method, a large β_c value, 590×10^{-30} esu, is obtained for the PANPAC chromophore because of the extended conjugation length. The PANTAC chromophore with the heterocyclic thiazole ring makes the β_c value, 1100×10^{-30} esu, even higher. In addition to an increase in β_c, red shifts in the UV/vis spectra are also observed in both polymers.

In the four-wave mixing experiments, the wavelength of the green laser lies at the peak of the UV/vis absorption spectrum of PANTAC/TDI and at the shoulder of PANPAC/TDI. The wavelength of the red laser locates at the shoulder of the former but at the valley of the latter. Although the β_c of the PANTAC chromophore is greater than that of the PANPAC chromophore, the maximum diffraction efficiency η_{max} of the PANTAC/TDI polymer is much lower than that of the PANPAC/TDI polymer, based on the same film thickness and the same writing and reading laser. It reveals that the stronger absorption of PANTAC/TDI film at 532 and 632 nm, compared with that of PANPAC/TDI film, offsets the merit from the large nonlinearity of the PANTAC chromophore. Both photorefractive (PR) films show the same trend that the maximum diffraction efficiencies of the PR films written/read by the green/red laser are much higher those written/read by the green/green laser. It is due to the stronger absorption of the reading beam and the diffracted beam at 532 nm than at 632 nm. It is also found that the maximum diffraction efficiency is strongly dependent on the film thickness. The maximum experimentally measured diffraction efficiencies of PANPAC/TDI and PANTAC/TDI are found at the film thickness of 23 and 15 μm, respectively, as they are written/read by the green/green laser, but the maximum experimentally measured diffraction efficiencies of both PR films are observed at the film thickness of 22 and 17 μm, respectively, as they are written/read by the green/red laser.

Similar influence is observed in the hologram recording experiment. The image recorded on the PANTAC/TDI film is darker and more vague than those written in the PANPAC/TDI film. PANPAC/TDI is a good hologram recording media since not only the images can be stored, erased, and updated repeatedly, but also the contrast and the brightness of the recorded hologram are greatly enhanced. It makes hologram recording by a single light source possible. Excellent holograms can be recorded and readout by a setup with lower cost.

Acknowledgment. The authors acknowledge financial support from the National Science Council of the R.O.C. under Grant No. NSC 87-2216-E009-002.

References and Notes

(1) Halvorson, C. B.; Kraabel, A. J.; Heeger, B. L.; Volodin, K.; Meerholz, B.; Sandalphon, K.; Peyghambarian, N. *Opt. Lett.* **1995**, *20*, 76.
(2) Vacar, D.; Heeger, A. J.; Volodin, B.; Kippelen, B.; Peyghambarian, N. *Rev. Sci. Instrum.* **1997**, *68*, 1119.
(3) Heanue, J. F.; Bashaw, M. C.; Hesselink, L. *Science* **1994**, *265*, 749.
(4) Lundquist, P. M.; Poga, C.; DeVoe, R. G.; Jia, Y.; Moerner, W. E.; Bernal, M. P.; Coufal, H.; Grygier, R. K.; Hoffnagle, J. A.; Jefferson, C. M.; Macfarlane, R. M.; Shelby, R. M.; Sinserbox, G. T. *Opt. Lett.* **1996**, *21*, 890.
(5) Volodin, B. L.; Sandalphon, K.; Meerholz, B.; Kippelen, N. V.; Kukhtarev, N.; Peyghambarian, N. *Opt. Eng.* **1995**, *34*, 2213.
(6) Zhang, Y., Spencer, C. A.; Ghosal, S.; Casstevens, M. K. *Appl. Phys. Lett* **1994,** *64*, 1908.
(7) Eich, M.; Reck, B.; Yoon, D. Y.; Willson, C. G.; Bjorklund, G. C. *J. Appl. Phys.* **1989**, *66*, 3241.
(8) Gelsen, O. M.; Bradley, D. D. C.; Murata, H.; Tsutsui, T.; Saito, S.; Ruhe, J.; Wegner, G. *Synth. Met.* **1991**, *41*, 875.
(9) Zhang, Y.; Cui, Y.; Prased, P. N. *Phys. Rev. B* **1992**, *46*, 9900.
(10) Donckers, M. C. J. M.; Silence, S. M.; Walsh, C. A.; Hach, F.; Burland, D. M.; Moerner, W. E.; Twieg, R. J. *Opt. Lett.* **1993**, *18*, 1044.
(11) Tamura, K.; Padias, A. B.; Hall, H. K., Jr.; Peyghambarian, N. *Appl. Phys. Lett.* **1992**, *60*, 1803.

(12) Kippelen, B.; Tamura, K.; Peyghambarian, N.; Padias, A. B.; Hall, H. K., Jr. *J. Appl. Phys.* **1993**, *74*, 3617.
(13) Li, J.; Lee, Y. J.; Yang, Y.; Kumar, J.; Tripathy, S. K. *Appl. Phys.* **1991**, *B53*, 279.
(14) Li, J.; Jeng, R. J.; Kamath, M.; Kumar, J.; Tripathy, S. K. *Mater. Res. Soc. Symp. Proc.* **1992**, *277*, 160.
(15) Yu, L.; Chen, Y. M.; Chan, W. K.; Peng, Z. H. *Appl. Phys. Lett.* **1994**, *64*, 2489.
(16) Sansome, M. J.; Teng, C. C.; East, A. J.; Kwiatek, M. S. *Opt. Lett.* **1993**, *18*, 1400.
(17) Ho, M. S.; Barrett, C.; Paterson, J.; Esteghamatian, M.; Natansohn, A.; Rochon, P. *Macromolecules* **1996**, *29*, 4613.
(18) Wong, K. Y.; Jen, A. K. Y.; Rao, V. P.; Drost, K. J. *J. Chem. Phys.* **1994**, *100*, 6818.
(19) Dirk, C. W.; Katz, H. E.; Schilling, M. L.; King, L. A. *Chem. Mater.* **1990**, *2*, 700.
(20) Cheng, L. T.; Tam, W.; Marder, S. R.; Stiegman, A. E.; Rikken, G.; Sprangler, C. W. *J. Phys. Chem.* **1991**, *95*, 10631.
(21) Wong, K. Y.; Jen, A. K. Y.; Rao, V. P. *Phys. Rev. A* **1994**, *49*, 3077.
(22) Jen, A. K. Y.; Rao, V. P.; Wong, K. Y.; Drost, K. J. *J. Chem. Soc., Chem. Commun.* **1993**, 90.
(23) Rao V. P.; Jen, A. K. Y.; Wong, K. Y.; Drost, K. J. *J. Chem. Soc., Chem. Commun.* **1993**, 1118.
(24) Rao, V. P.; Jen, A. K. Y.; Chandrasekhar, J.; Namboothiri, I. N. N.; Rathna, A. *J. Am. Chem. Soc.* **1996**, *118*, 12443.
(25) Ouder, B. L.; Chemla, D. S. *J. Chem. Phys.* **1977**, *66*, 2664.
(26) Chen, L. T.; Tam, W.; Marder, S. R.; Stiegman, A. E.; Rikken, G.; Sprangler, C. W. *J. Phys. Chem.* **1991**, *95*, 10643.
(27) Dulcic, A.; Flytzanis, C.; Tang, C. L.; Pepin, D.; Fitzon, M.; Hoppiliard, Y. *J. Chem. Phys.* **1981**, *74*, 1559.
(28) Morley, J. D.; Docherty, V. J.; Pugh, D. *J. Chem. Soc., Perkin Trans. 2* **1987**, *1351*, 1357.
(29) Clays, K.; Hendrickx, E.; Triest, M.; Verbiest, T.; Persoons, A.; Dehu, A. C.; Bredas, J. L. *Science* **1993**, *262*, 1419.
(30) Laidlaw, W. M.; Denning, R.G.; Verbiest, T.; Chauchard, E.; Persoons, A. *Nature* **1993**, *363*, 58.
(31) Pauley, M. A.; Wang, C. H.; Jen, A. K. Y. *J. Chem. Phys.* **1995**, *102*, 6400.
(32) Flipse, M. C.; de Jonge, R.; Woudenberg, R. H.; Marsman, A. W.; Van Walree, C. A.; Jenneskens, L. W. *Chem. Phys. Lett.* **1995**, *245*, 297.
(33) Hsu, C. C.; Huang, T. H.; Zang, Y. L.; Ling, J. L.; Cheng, Y. Y.; Lin, J. T.; Wu, H. H.; Wang, C. H.; Kuo, C. T.; Chen, C. H. *J. Appl. Phys.* **1996**, *80*, 5996.
(34) Tamura, K.; Padias, A. B.; Hall, H. K., Jr.; Peyghambarian, N. *Appl. Phys. Lett.* **1992**, *60*, 1803.
(35) Zhang, Y. D.; Wada, T.; Wang, L.; Aoyama, T.; Sasabe, H. *Chem. Commun.* **1996**, 2325.
(36) Kogelnik, H. *Bell Syst. Technol. J.* **1969**, *48*, 2909.

MA981922D